A New Analytical Approach for Dynamic Modeling of Passive Multicomponent Cooling Systems

A. Gholami
Laboratory for Alternative Energy Conversion (LAEC),
School of Mechatronic Systems Engineering,
Simon Fraser University,
Surrey, BC V3T 0A3, Canada

M. Ahmadi
Laboratory for Alternative Energy Conversion (LAEC),
School of Mechatronic Systems Engineering,
Simon Fraser University,
Surrey, BC V3T 0A3, Canada

M. Bahrami[1]
Laboratory for Alternative Energy Conversion (LAEC),
School of Mechatronic Systems Engineering,
Simon Fraser University,
Surrey, BC V3T 0A3, Canada
e-mail: mbahrami@sfu.ca

A new one-dimensional thermal network modeling approach is proposed that can accurately predict transient/dynamic temperature distribution of passive cooling systems. The present model has applications in variety of electronic, power electronic, photonics, and telecom systems, especially where the system load fluctuates over time. The main components of a cooling system including: heat spreaders, heat pipes, and heat sinks as well as thermal boundary conditions such as natural convection and radiation heat transfer are analyzed, analytically modeled and presented in the form of resistance and capacitance (RC) network blocks. The present model is capable of predicting the transient/dynamic (and steady state) thermal behavior of cooling system with significantly less cost of modeling compared to conventional numerical simulations. Furthermore, the present method takes into account system "thermal inertia" and is capable of capturing thermal lags in various components. The model is presented in two forms: zero-dimensional and one-dimensional which are different in terms of complicacy. A custom-designed test-bed is also built and a comprehensive experimental study is conducted to validate the proposed model. The experimental results show great agreement, less than 4.5% relative difference in comparison with the modeling results. [DOI: 10.1115/1.4027509]

Keywords: thermal management, passive cooling system, RC network modeling, dynamic loading

1 Introduction

The continued growth in performance and functionality of telecom, microelectronic, and photonics systems combined with miniaturization trend in the industry have resulted in a significant increase in heat generation rates [1–3], and presents a great challenge to thermal engineers. A number of failure mechanisms in electronic devices such as intermetallic growth, metal migration, and void formation are directly linked to thermal effects. According to Arrhenius law, the rate of these failures is approximately doubled with every 10 °C increase in the operating temperature of the device. In fact, more than 65% of system failures have thermal roots [4]. In addition, the fluctuations in the system loads can adversely impact the efficiency and reliability by forming temporary hotspots, thus thermal stresses. In optoelectronics, photonics, and microelectronics, the ability to understand, predict, and possibly minimize the thermal stresses such as brittle fracture, thermal fatigue, thermal shock, and stress corrosion is of crucial importance [5,6]. Electronics and telecommunication devices mainly operate in transient or pulsed mode, mainly in applications such as: AC/DC rectifiers, uninterruptible power supply modules, and inverters. There are different cooling techniques to dissipate the heat from these systems. Among them, passive cooling methods are widely preferred since they provide low-cost, nonparasitic power, quiet operation, and reliable cooling solutions.

One method to model transient thermal systems is using thermal RC networks analog to electrical circuits [7]. In this analogy, voltage and current stand for temperature and heat flow rate, respectively. Such RC network models range from simple ones which only consider the most important thermal phenomena to complicated networks which include the details of the cooling system.

Steady state thermal resistance network models have been extensively studied in the literature, see e.g., Refs. [8–16]. There are also a number of studies that include the capacitive behavior of the components to account for transient heat transfer. Barcella et al. [17] presented a RC modeling method for architecture-level simulation of very-large-scale-integration chips. Following Barcella's work, Stan et al. [18] introduced a thermal RC modeling approach applicable to microprocessor dies and the attached heat sink. Magnone et al. [19] and Cova et al. [20] presented Cauer RC network model for transient conduction inside silicon power devices and power device assemblies. A thermal RC network model was introduced by López-Walle et al. [21] that was capable of modeling heat transfer in micro thermal actuators for both static and dynamic modes. Miana and Cortés in Refs. [22] and [23] presented a transient thermal network modeling for prediction of temperature map in multiscale systems subjected to convection at one end. The method was based on dividing the geometry into isothermal elements according to characteristic length and length scale obtained by scale analysis. The RC network modeling concept also has been used in transient modeling of building solar gain [24–26]. The above studies are mostly limited to component-level modeling and component temperature map prediction and no system-level analysis of the effect of thermal inertia and dynamic loadings on the performance of the cooling systems is performed. Therefore, a comprehensive and robust yet fast and simple approach for transient thermal network (RC) modeling of multicomponent systems that can cover a broad range of applications such as building cooling system, automobile industry, and aviation is needed. In this study an efficient compact thermal network model is proposed that can accurately predict real-time transient and steady state behavior of electronic, power electronic and photonic systems.

The present RC thermal model is capable of covering the entire range of cooling solutions from module/component level to system level with any number of components. To apply the thermal

[1]Corresponding author.
Contributed by the Electronic and Photonic Packaging Division of ASME for publication in the Journal of Electronic Packaging. Manuscript received January 27, 2014; final manuscript received April 18, 2014; published online May 12, 2014. Assoc. Editor: Gongnan Xie.

 Copyright © 2014 by ASME

Downloaded From: http://turbomachinery.asmedigitalcollection.asme.org/ on 04/13/2015 Terms of Use: http://asme.org/terms

RC model to a system, first, all the components should be modeled individually by RC. Then, based on the heat flow, an equivalent thermal circuit should be formed using these RC blocks. One major advantage of the proposed thermal network method is its simplicity, i.e., the transient behavior of the system under various operating and load conditions can be simulated rather easily without using complicated and time consuming numerical solutions.

The proposed RC model is focused on passive cooling systems; however, the same approach can be used for active cooling systems. The considered passive system includes heat spreader, heat pipe, and naturally cooled heat sink. The model is developed at two complicacy levels of zero-dimensional (0D) and one-dimensional (1D) which support both transient and steady state conditions. The proposed model is capable of simulating any arbitrary loading and operating scenarios. A custom-designed test-bed is developed and several passive cooling systems are built and tested. The model is successfully validated with experimental data and an excellent agreement between the modeling results and experimental data is observed.

2 Model Development

In general, a passive multicomponent cooling system includes the following main components: (i) heat spreaders; (ii) heat pipes; and (iii) heat sinks. A schematic of a typical passive cooling system is shown in Fig. 1.

Every component on the heat transfer path causes a temperature drop, i.e., resistance to the heat flow. This temperature drop is a function of geometry (dimensions and shape), thermophysical properties of the component as well as the heat flow rate. The ratio of temperature drop over the rate of heat flow is known as thermal resistance [7].

$$R = \frac{\Delta T}{Q} \quad (1)$$

where ΔT is temperature drop and Q is the heat transfer rate. System components also have thermal inertia acting as thermal capacitors that store or release heat during transient operation. This capacitive characteristic results in a "thermal lag" in the system response to variations, e.g., boundary conditions or thermal load. In addition to the components, there are also some thermal phenomena at the system boundaries and components' interface, such as natural convection, radiation and thermal contact resistance which should be considered as resistances against the heat flow. It should be noted, no capacitor has to be considered for the boundary phenomena as they do not show any thermal mass effect.

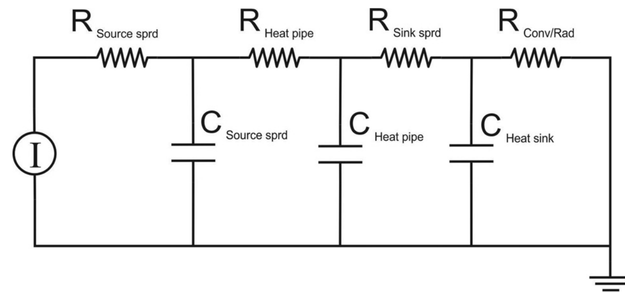

Fig. 2 One-dimensional RC model of the passive cooling system shown in Fig. 1 including: heat source, heat spreader at the heat source, heat pipe, and naturally cooled heat sink

Knowing thermal resistances and capacitances, an RC model can be constructed and analyzed rather simply using software such as MATLAB, LTSPICE, or SAPWIN, which enables simulation and accurate prediction of the thermal behavior of any cooling system over time at each desired point in the system under any arbitrary operating scenario. The computation time depends highly on the level of complicacy of the system as well as the processor being used which differs for different applications. The approximate time to solve a 10-component system for 2 h of real operation time using a Core i7 computer is around 5 s. To calculate the resistances and capacitances in an RC model, all the dimensions and thermal properties of the components as well as boundary conditions (e.g., ambient temperature) should be known. For the radiation thermal resistance, emissivity of the radiant surface should be known as well.

In Secs. 2.1 and 2.2, two general network models are presented to predict the behavior of thermal systems under both transient and steady state conditions. The first one which is called 1D model is more comprehensive, accurate, and accommodates more details whereas the second model which is referred to as 0D and is a simplified version of the 1D model, is less accurate but faster. Contact resistance due to comparatively small value is neglected in both models; however, it can be included in systems where contact resistance is important.

2.1 One-Dimensional Thermal Network Model. Here, the thermal network model of a typical passive cooling system, shown in Fig. 1, is studied. The present model can be extended to any other passive (or active) cooling system with any number of components. The proposed 1D RC model, for the system shown in Fig. 1, is demonstrated in Fig. 2.

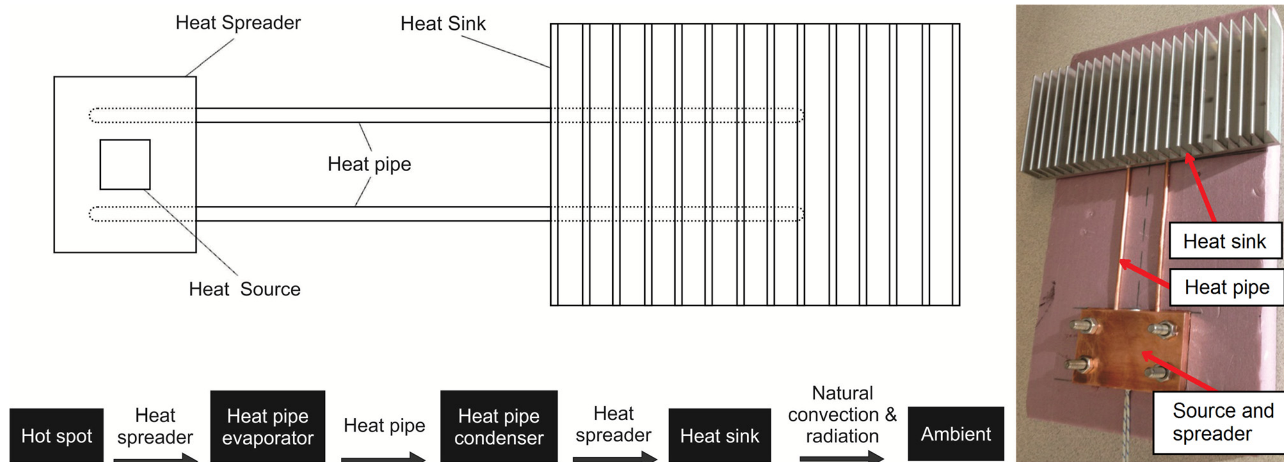

Fig. 1 Left: schematic and block diagram of a typical passive cooling system; right: a modeled passive system test-bed

Downloaded From: http://turbomachinery.asmedigitalcollection.asme.org/ on 04/13/2015 Terms of Use: http://asme.org/terms

The capacitance of each component can be calculated using Eq. (2) which is the summation of all subcomponents' capacities

$$C = \sum_i (mc_{\mathrm{p}})_i = \sum_i (\rho c_{\mathrm{p}} V)_i \tag{2}$$

where m is the mass of each part, c_{p} is the thermal capacity, and ρ and V are the density and the volume of each part, respectively. However, the approach to define the resistance of each component is different. In Secs. 2.1.1–2.1.4, a resistance model for each component is developed.

2.1.1 Heat Spreader Resistance. Most of heat spreaders are rectangular in shape with rectangular hot/cold spots on the top and bottom surfaces. Figure 3(*a*) shows a schematic of a rectangular heat spreader with multiple hot/cold spots on its faces. The dimensions and the location of heat sources are depicted in Fig. 3(*b*).

The thermal resistance of such plates is defined as follows:

$$R = \frac{\dfrac{1}{A_{\mathrm{sources}}} \displaystyle\sum_{\mathrm{Sources}} \int_{Y_i - \frac{b_i}{2}}^{Y_i + \frac{b_i}{2}} \int_{X_i - \frac{a_i}{2}}^{X_i + \frac{a_i}{2}} T_{\mathrm{Sources}} dxdy - \dfrac{1}{A_{\mathrm{Sinks}}} \displaystyle\sum_{\mathrm{Sinks}} \int_{Y_j - \frac{b_j}{2}}^{Y_j + \frac{b_j}{2}} \int_{X_j - \frac{a_j}{2}}^{X_j + \frac{a_j}{2}} T_{\mathrm{Sinks}} dxdy}{\left| \displaystyle\iint_{\mathrm{Sources/Sinks}} q_i dxdy \right|} \tag{3}$$

In order to calculate the average temperatures in Eq. (3), temperature distribution inside the heat spreader is needed. The author has developed an analytical solution for temperature distribution inside anisotropic heat spreaders with arbitrary heat flux on the hotspots in a different study [27]. The final results are presented in the Appendix; more details can be found in Ref. [27].

For irregular and nonrectangular heat spreaders, one may approximate the heat spreader geometry with the equivalent rectangular block to estimate the spreading resistance. One such example is the rectangular heat spreader used in the experimental test setup of this study which sandwiches one heat pipe and one cylindrical heater, Fig. 4(*a*). For this case, the heat spreader is approximated with two separate plates which are thermally connected in parallel. The hotspots are the projected areas of the cylinders, heat pipe, and heater on the surface, Fig. 4(*b*). With this approximation the equivalent resistance network of the spreaders will be two identical single plate resistances working in parallel; see Fig. 4(*c*), which can be readily calculated using Eq. (3).

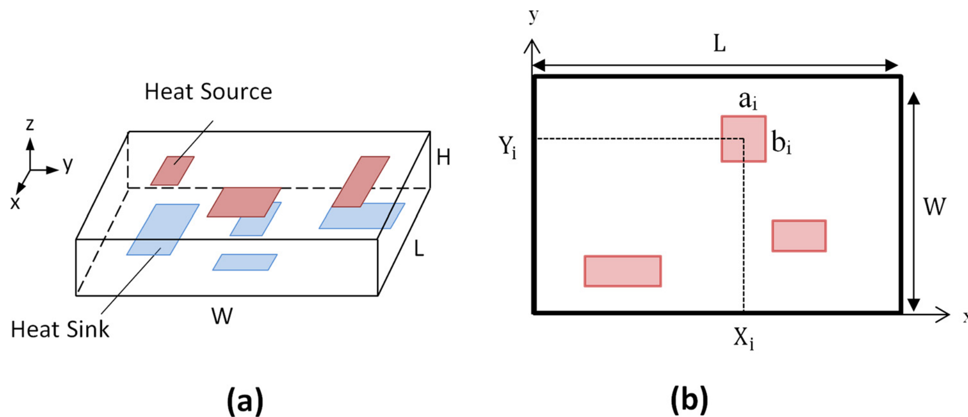

Fig. 3 Schematic of a rectangular spreader with multiple hotspots on the top and bottom surfaces (*a*) and size and location of the hotspots (*b*)

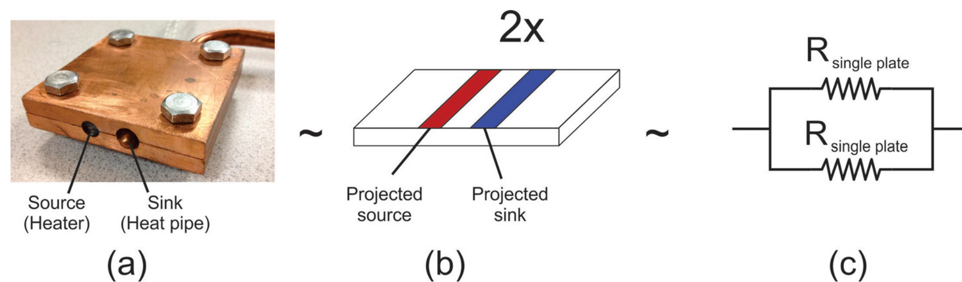

Fig. 4 Heat spreaders of the present experimental test setup, sandwiching one heat pipe and one cylindrical electric heater: (*a*) real geometry, (*b*) approximated heat spreader geometry, and (*c*) equivalent thermal resistance network model

Downloaded From: http://turbomachinery.asmedigitalcollection.asme.org/ on 04/13/2015 Terms of Use: http://asme.org/terms

2.1.2 Heat Pipe Resistance. In a heat pipe, heat is transported through three paths: (i) inner hollow, through conduction and convection, (ii) wick, through conduction, and (iii) wall, through conduction. Figure 5 shows the thermal resistance circuit of a heat pipe.

In Fig. 5, the axial resistances have comparatively large values, so they can be assumed as open circuit. On the other hand, the vapor resistance is very small and can be assumed as short circuit [13,28,29].

Applying these simplifications and considering the thermal storage of a heat pipe, thermal network of a heat pipe can be represented as shown in Fig. 6.

The radial thermal resistance for a cylinder wall with inner and outer radiuses of r_1 and r_2 and length of L with thermal conductivity of k is

$$R_r = \frac{\ln\left(\frac{r_2}{r_1}\right)}{2\pi k L} \tag{4}$$

Thus, the resistance of a cylindrical heat pipe is simply the summation of all the resistances shown in Fig. 6

$$R_{\mathrm{HP}} = \frac{L_e + L_c}{2\pi L_e L_c}\left(\frac{\ln\left(\frac{r_{\mathrm{out}}}{r_{\mathrm{wall}}}\right)}{k_{\mathrm{wall}}} + \frac{\ln\left(\frac{r_{\mathrm{wall}}}{r_{\mathrm{wick}}}\right)}{k_{\mathrm{wick}}}\right) \tag{5}$$

where r_{out} is the pipe outer radius, r_{wall} and r_{wick} are inner radii of the wall and the wick, L_e and L_c are the length of the evaporator and the condenser sections, and k_{wall} and k_{wick} are thermal conductivities of the wall and effective thermal conductivity of the wick, respectively. Effective thermal conductivity of two commonly used types of wick structure is defined as below [12,28]

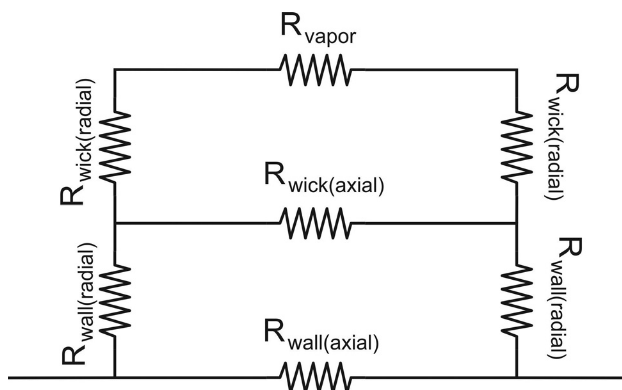

Fig. 5 Thermal resistance network model of heat pipe (steady state)

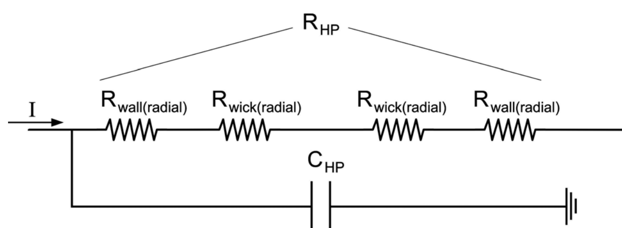

Fig. 6 Simplified thermal network model of heat pipe

$$k_{\mathrm{wick}} = \frac{k_l[(k_l + k_s) - (1-e)(k_l - k_s)]}{[(k_l + k_s) + (1-e)(k_l - k_s)]} \quad \text{wrapped screen wick}$$
$$k_{\mathrm{wick}} = \frac{k_s[2 + (k_l/k_s) - 2e(1-(k_l/k_s))]}{[2 + (k_l/k_s) + e(k_l/k_s)]} \quad \text{sintered wick} \tag{6}$$

where k_l and k_s are thermal conductivities of liquid and wick material, respectively, and e is the wick porosity. The capacitance of the heat pipe is also calculated using Eq. (2).

2.1.3 Heat Sink Spreading Resistance. There are different types of heat sinks in terms of fin shape and dimensions such as continuous rectangular fin, interrupted fin, pin fin, and microchannel heat sinks with different fin patterns [30–34]. The following model is presented for typical continuous rectangular finned heat sink but can easily be applied to other types of fin. To use the present 1D model, we should assume a uniform temperature for heat sinks. This assumption is not far from reality for most engineering applications; however, it may introduce some inaccuracy in the model. As the heat enters from the heat sink base to be transferred to the surroundings, it encounters a spreading resistance in the base, which causes a temperature drop inside the heat sink. Uniform temperature assumption on the outer surface implies that the fins thermal resistance is negligible compared to the base plate resistance. Neglecting the resistance of the fins simplifies the heat sink's thermal resistance into the resistance of a rectangular block whose thickness is equal to the thickness of the base plate. In this block, heat sources are the projected area of the hotspots on the back face, and heat sinks are a series of alternate rectangular strips with length of the block width, and widths of fin thickness and fin spacing which cover the whole surface of block, as shown in Fig. 7. Assuming a uniform convective heat transfer coefficient over the heat sink surface, the dissipated heat through the strips on the equivalent block can be determined using its corresponding area in the real heat sink. For a heat sink with n_f fins, fin spacing of s, fin thickness of t, and fin depth of p, the heat transfer will be

$$Q_{\mathrm{fin}} = \frac{2p + t}{2n_f p + L} Q_{\mathrm{in}} \quad \text{one fin strip}$$
$$Q_{\mathrm{base}} = \frac{s}{2n_f p + L} Q_{\mathrm{in}} \quad \text{one base strip} \tag{7}$$

Having the heat sink simplified to the above-mentioned geometry which is a multihotspot rectangular heat spreader, the spreading resistance can be calculated using the approach explained in Sec. 2.1.1.

2.1.4 Convective/Radiative Resistance. On the surface of a heat sink, heat is dissipated to the ambient through two parallel mechanisms: (i) natural convection and (ii) radiation [35]. Using the definition of the thermal resistance, Eq. (1), the surface thermal resistance of a heat sink can be defined as

$$R = \frac{\Delta T}{Q_{\mathrm{convection}} + Q_{\mathrm{Radiation}}} \tag{8}$$

where ΔT is the temperature difference between the surface of the heat sink and the ambient. The amount of convective heat transfer is the summation of heat transfers from the fins and the base

$$Q_{\mathrm{Convection}} = h_f A_f \Delta T + h_b A_b \Delta T \tag{9}$$

where the subscripts f and b refer to "fin" and "base plate," respectively. The following correlations are used for calculating the convective heat transfer coefficient in rectangular finned heat sinks [35]:

$$h_b = \frac{k}{L} 0.59 \mathrm{Ra}_L^{0.25} \quad \text{Single plate (base plate)} \tag{10}$$

Downloaded From: http://turbomachinery.asmedigitalcollection.asme.org/ on 04/13/2015 Terms of Use: http://asme.org/terms

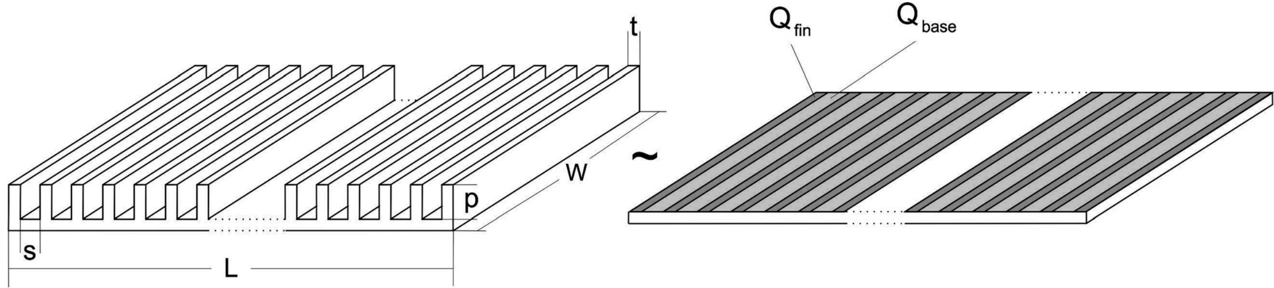

Fig. 7 Rectangular finned heat sink and its base rectangular shape equivalent spreader

$$h_f = \frac{k}{s}\left[\frac{576}{\left(\frac{\mathrm{Ra}_s s}{L}\right)^2} + \frac{2.873}{\left(\frac{\mathrm{Ra}_s s}{L}\right)^{0.5}}\right]^{-0.5} \quad \text{Parallel plates (fins)} \tag{11}$$

where

$$\mathrm{Ra}_x = \frac{g\beta}{\nu\alpha}(T_s - T_{\mathrm{amb}})x^3 \tag{12}$$

In the above correlations, L and s are fin length and fin spacing of the heat sink, respectively. Other types of heat sinks can be modeled using a similar approach.

For radiation heat transfer, the following correlation is used [35]:

$$Q_{\mathrm{Radiation}} = \sigma\left(T_s^4 - T_{\mathrm{amb}}^4\right)\left(\sum_i \frac{1}{\frac{1-\varepsilon_i}{A_i\varepsilon_i} + \frac{1}{A_iF_{i\infty}}}\right) \tag{13}$$

where σ, ε, and F are Stefan–Boltzmann coefficient, emissivity, and the view factor of surface i, respectively. The view factor of a single duct surface of heat sink for comparatively small fin aspect ratios can be calculated using the following approximation:

$$F = \frac{s}{s+2p} \tag{14}$$

Substituting the correlations for both convective and radiative heat transfers, Eqs. (9) and (13), into the resistance definition, Eq. (8), the following relationship for the thermal resistance of a rectangular heat sink is derived:

$$R = \frac{1}{h_fA_f + h_bA_b + \sigma\left(T_s^2 + T_{\mathrm{amb}}^2\right)(T_s + T_{\mathrm{amb}})\left(\sum_i \frac{1}{\frac{1-\varepsilon_i}{A_i\varepsilon_i} + \frac{1}{A_iF_{i\infty}}}\right)} \tag{15}$$

Equation (15) shows that the resistance is a function of thermophysical properties as well as the temperature of both heat sink and the environment.

2.2. Zero-Dimensional Thermal Network Model. In the systems where the amount of components resistance is smaller than the convective resistance on the heat sink by an order of magnitude or higher, the whole system can be treated as a lumped body with no resistance. According to Ref. [35], these criteria can be quantified and stated in the form of Biot number criteria. The lumped system analysis is applicable if $Bi \leq 0.1$ [35]

$$Bi = \frac{hL_c}{k} \tag{16}$$

where h is the convective heat transfer coefficient, k is thermal conductivity of the body, and L_c is the characteristic length which is commonly defined as the volume of the body divided by the convection surface area. For systems with Biot smaller than 0.1, the corresponding RC circuit consists of one capacitance and one convective–radiative resistance, Fig. 8.

In Fig. 8, the resistance is calculated according to Sec. 2.1.4 and the capacitance is the summation of the capacity of all the components of the system, calculated using Eq. (2).

3 Experimental Study

To validate the present model, a custom-designed experimental test setup is built. The test setup is a passive cooling mechanism consisting of two electric cartridge heaters with the maximum rated powers of 40 W supplied by OMEGA (Toronto, ON). Heaters are connected to a naturally cooled rectangular finned heat sink via round heat pipes (Fig. 9). They are sandwiched between copper plates which work as heat spreaders and are powered by an adjustable AC power supply (VARIAC, China). The uncertainty of power supply reported by the company is ± 0.1W. To monitor and log the temperature data, T-type thermocouples with uncertainty of $\pm 0.5°C$ in conjunction with National Instrument DAQ system are used. Dimensions and thermal properties of the testbed components are listed in Table 1.

3.1 Test Procedure. Different step and oscillatory loading scenarios are imposed to the cooling system by heaters and the temperature data is monitored and logged throughout the experiment. Each test is carried out for the transition time starting from the initial equilibrium state in which all the components are in equilibrium with the ambient, to the final steady state. At the steady state, the temperature becomes either statically or

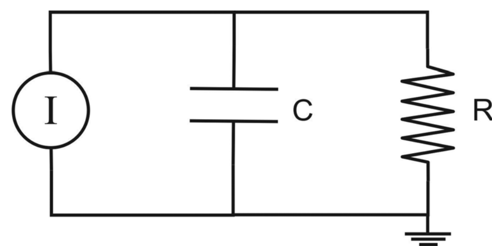

Fig. 8 A 0D RC network model of the passive cooling system shown in Fig. 1

Downloaded From: http://turbomachinery.asmedigitalcollection.asme.org/ on 04/13/2015 Terms of Use: http://asme.org/terms

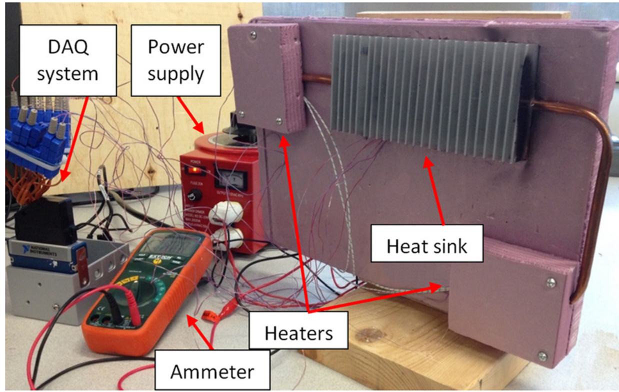

(a)

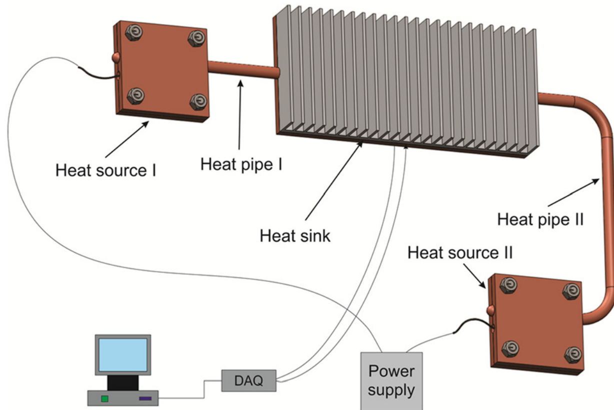

(b)

Fig. 9 **(*a*) Test-bed and (*b*) schematic of the two-path experimental test-bed**

"dynamically" steady depending on the load profile of the heaters. For temperature measurement, 16 thermocouples are attached to different locations in the test-bed to keep track of temperature variations at important locations. To investigate the thermal behavior of the system in different load cycles and validate the present 0D and 1D models, the experiments are conducted for the following two different loading scenarios:

(I) Static loading; each heater has a constant power.
(II) Dynamic loading; each heater has a cyclic heat load profile.

Applying the methodology described earlier, the present 1D RC model of the test-bed is shown in Fig. 10. For the 0D RC model, the RC network has the form shown in Fig. 8 ($Bi \simeq 0.02$). The values of the components are listed in Table 2.

3.2 Model Validation. To validate the proposed models, experimental data recorded for different heating scenarios are plotted and compared with their corresponding model simulations. Three important locations, two on the heat sources and one on the heat sink, are chosen as benchmarks for comparison and validation. In Fig. 11, the temperature at these three spots are compared with the 1D as well as the 0D model for the static loading of 10 W for heater I and 14 W for heater II.

As the 0D model only provides one temperature for the whole test-bed as a lumped mass, it is not capable to detect the temperature difference between the heat sinks and heat sources. Therefore, in Fig. 11, it can be seen that the 0D model captures the heat sink temperature reasonably well with less than 2% relative difference. However, it is not capable of predicting other components temperature such as heat sources. The present 1D model, however, is capable of accurately predicting temperatures at different spots as it considers the thermal resistance between the components. The maximum relative difference with the experimental data with the 1D model is approximately 4%. Figure 12 depicts another static loading case (Heater I, 5 W and heater II, 9 W) in which again the heat sink temperature is accurately predicted by both 0D and 1D

Table 1 **Test-bed thermophysical specifications**

	Spreader I	Spreader II	Heat pipe I	Heat pipe II	Heat sink
Material	Copper	Copper	Copper	Copper	Aluminum
Length (mm)	63	63	$L_{HP} = 200$ $L_e = 30$ $L_c = 30$	$L_{HP} = 300$ $L_e = 30$ $L_c = 30$	185
Width (mm)	63	63	—	—	86
Thickness (mm)	6	6	$t_{wall} = 0.8$ $t_{wick} = 1.2$	$t_{wall} = 0.8$ $t_{wick} = 1.2$	$t_{base} = 5$ $t_{fin} = 2$
Diameter (mm)	—	—	$D_{out} = 8$	$D_{out} = 8$	—
Fin depth (mm)	—	—	—	—	17
Fin spacing (mm)	—	—	—	—	6
Thermal conductivity (W/m·K)	400	400	$k_{copper} = 400$ $k_{wick} = 50$	$k_{copper} = 400$ $k_{wick} = 50$	120
Density (kg/m^3)	8960	8960	8960	8960	2700
Specific heat (J/kg·K)	386	386	386	386	900

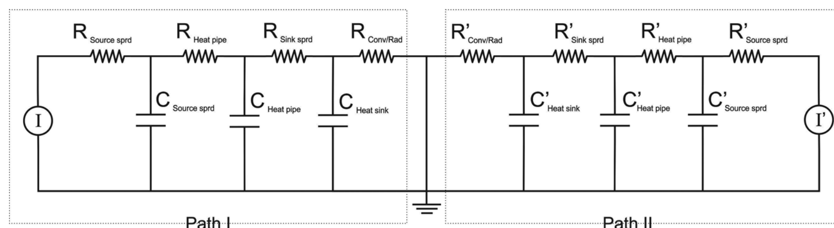

Fig. 10 **One-dimensional model of the two-path experimental test-bed**

Downloaded From: http://turbomachinery.asmedigitalcollection.asme.org/ on 04/13/2015 Terms of Use: http://asme.org/terms

Table 2 **Component values of the RC models of the two-path experimental test setup**

	Resistance (K/W)				Capacitance (J/K)		
	Heat source spreader	Heat pipe	Heat sink spreader	Convection/radiation	Heat source spreader	Heat pipe	Heat sink
1D (path I)	0.052	0.014	0.19	1.5	140	18	350
1D (path II)	0.052	0.014	0.19	1.5	140	27	350
0D	$R_{total} = 1.5$				$C_{total} = 1025$		

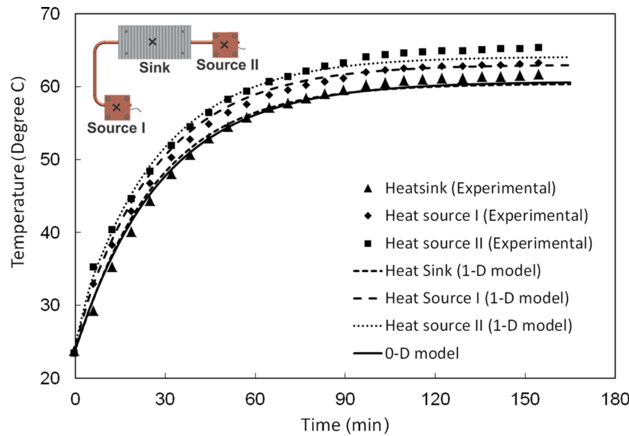

Fig. 11 Zero-dimensional model validation with experimental data at three locations of heat sink and two heat sources for the heating scenario of constant 14 W for heater I and 10 W for heater II

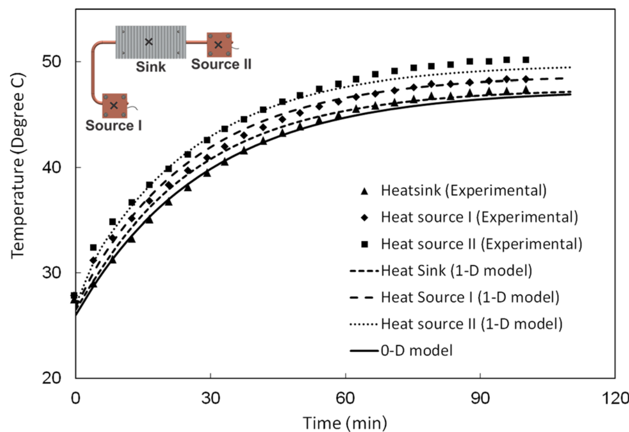

Fig. 12 Zero-dimensional model validation with experimental data at three locations of heat sink and two heat sources for the heating scenario of constant 9 W for heater I and 5 W for heater II

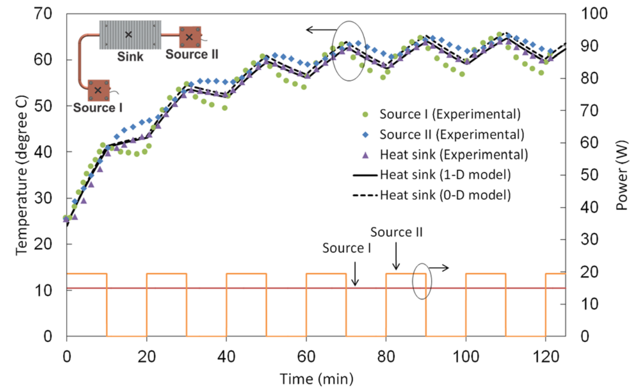

Fig. 13 Comparison of 0D model with experimental temperature of three different locations on the test-bed for the applied dynamic loading of shown in the figure

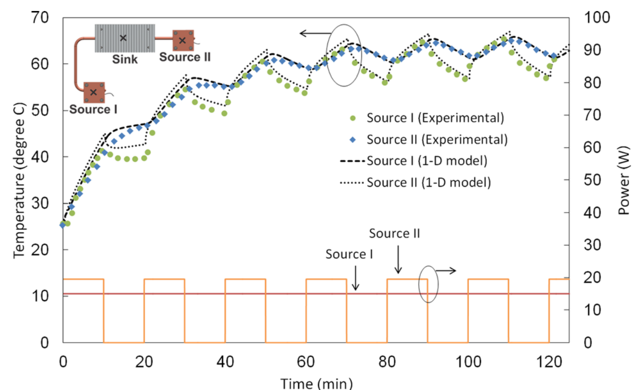

Fig. 14 One-dimensional model validation with experimental data at two heat source locations for the imposed dynamic loading shown

models whereas the temperature of the heat sources can only be predicted by the 1D model.

Figures 11 and 12 indicate that the temperature of other locations in the test-bed has almost the same trend as the temperature of the heat sink with a small offset. It can be interpreted that for cases with no sharp variation in heat source power, the 0D model is sufficient if the purpose is only to predict an estimation of the system temperature. Obviously, for variable loading situations in which the internal thermal resistances and thermal inertia become important, a 0D model cannot provide detailed information.

The following two dynamic loading scenarios are selected arbitrarily: (i) heater I with a constant heat generation of 13 W and heater II with a pulsating heat generation with a maximum of 20 W and a minimum of 0 and the period of 20 min and (ii) heater I with a two-step pulsating heat generation with the profile shown in Fig. 15 and heater II turned off.

Figure 13 presents the measured temperatures over time at three specified spots as well as the both models results for heat sink temperature. Both 0D and 1D models have predicted the heat sink temperature accurately. As it is seen, unlike the static form of loading, the shape of temperature variation for dynamic loading is different at various locations. These differences are due to thermal inertia effects and the 0D model is unable to detect them. The 1D model results for the two heat sources are shown in Fig. 14. It is indicated that the 1D model performs very good and captures the trend of the temperature fluctuation at the two hotspots. The relative difference between the model and experimental data in this case is less than 4%.

The comparison for the second scenario is shown in Figs. 15 and 16. This loading scheme represents the worst case in terms of fluctuation and thermal inertia effect on the thermal behavior of the system. As it is seen in Fig. 15, both models capture the heat sink temperature very well. It is worth noting that the temperature variation at the pulsating heater is very sharp while at the other heat source the temperature fluctuates much smoother with a lag in responding to the power changes, which is due to the damping

Downloaded From: http://turbomachinery.asmedigitalcollection.asme.org/ on 04/13/2015 Terms of Use: http://asme.org/terms

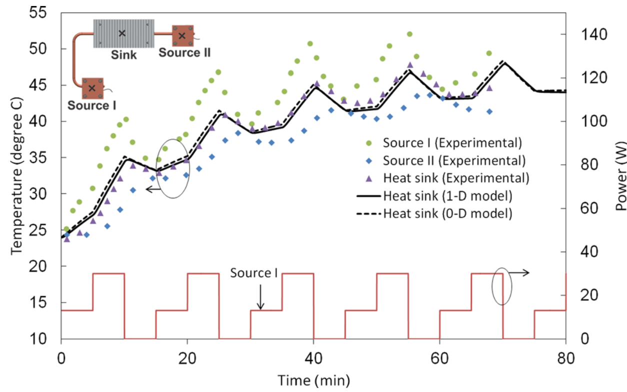

Fig. 15 Comparison of 0D model with experimental temperature of three different locations on the test-bed for the imposed dynamic loading shown in the figure

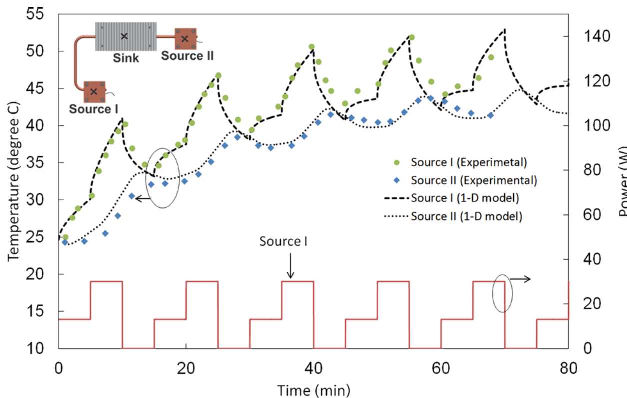

Fig. 16 One-dimensional model validation with experimental data at two heat source locations for the imposed dynamic loading shown in the figure

effect caused by thermal inertia of the system components. This effect is completely captured by the 1D model and the results for these two temperatures are plotted and compared with our experimental data in Fig. 16. The maximum relative difference between the model and experimental data is approximately 4.5%.

4 Summary and Conclusion

A new analytical methodology is developed that can accurately predict the dynamic thermal responses of electronic, power electronic, telecom cooling systems. The passive cooling solution components are modeled including: heat spreaders, heat pipes, and heat sinks. The compartments are modeled individually with a network of resistances and capacitances which represents the transient thermal behavior of that compartment. Then the corresponding R and C blocks are appropriately assembled to form a network to represent the thermal system. Compact relationships are presented for the resistances and capacitance of the considered passive compartment. Convection and radiation heat transfer on the heat sink are also modeled as a resistance in the model. By analyzing the equivalent thermal circuit, the model is capable of predicting the temperature distribution of the system in both transient and steady state for any loading scenario. Two versions of the present RC model are proposed: (i) 0D that is much simpler but provides a rough estimate of system thermal behavior and is applicable only for Biot numbers smaller than 0.1 and (ii) 1D: a more complicated which provides more details and is valid for all range of Biot. To validate the present RC model, a two-path passive cooling test-bed consisting of two heaters connected to a heat sink using two heat pipes and two spreaders is built. The test-bed is used for different dynamic thermal loading scenarios; and the temperatures at 16 locations are measured and recorded. The comparison between the proposed model and the experimental data shows an excellent agreement with relative difference of approximately 4.5%.

Acknowledgment

The author gratefully acknowledges the financial support of the Natural Science and Engineering Research Council of Canada (Grant No. 31-614094) and Alpha Technologies-Sponsored Research (NSERC-EGP 420143-11 Alpha Tech.).

Nomenclature

A, B = temperature solution coefficients
a_i, b_i = source or sink's length and width (m)
$A_{\text{source/sink}}$ = sources or sinks area (m^2)
C = capacitance (J/K)
c_p = specific heat capacity (J/kg·K)
e = porosity
F = view factor
g = gravity (m/s^2)
h = convective heat transfer coefficient (W/m^2·K)
k = thermal conductivity (W/m·K)
L = length (m)
L_e, L_c = heat pipe evaporator and condenser length (m)
m, n = number of eigenvalues
m_i = mass of component I (kg)
n_f = number of heat sink fins
p = fin depth (m)
q = heat flux (W/m^2)
Q = heat flow (W)
r = radius (m)
R = resistance (K/W)
Ra = Rayleigh number
s = fin spacing (m)
s_{ij} = auxiliary coefficients of temperature solution
T = temperature (K)
V_i = volume of component I (m^3)
W = width (m)
X_i, Y_i = source/sink center coordinates (m)
α = thermal diffusivity (m^2/s)
β = thermal expansion coefficient (1/K)
ε = width to length ratio of plate
ε_H = height to length ratio of plate
ε_i = emissivity of surface i
θ = dimensionless temperature
κ_x, κ_y = in-plane to through-plane thermal conductivity ratio in x and y directions
λ, δ, β = temperature solution eigenvalues
ν = kinematic viscosity (m^2/s)
σ = Stefan–Boltzmann constant (W/m^2·K^4)

Appendix

The following is the final solution for temperature distribution inside an anisotropic rectangular plate with multiple hot/cold spots on the top and bottom surfaces:

$$\theta = A_0 z^* + \sum_{m=1}^{\infty} \cos(\lambda \kappa_x x^*) \times [A_m \cosh(\lambda z^*) + B_m \sinh(\lambda z^*)] + \sum_{n=1}^{\infty} \cos(\delta \kappa_y y^*) \times [A_n \cosh(\delta z^*) + B_n \sinh(\delta z^*)] + \sum_{n=1}^{\infty}\sum_{m=1}^{\infty} \cos(\lambda \kappa_x x^*) \cos(\delta \kappa_y y^*) \times [A_{mn} \cosh(\beta z^*) + B_{mn} \sinh(\beta z^*)]$$

Downloaded From: http://turbomachinery.asmedigitalcollection.asme.org/ on 04/13/2015 Terms of Use: http://asme.org/terms

where λ, δ, and β are eigenvalues and A and B coefficients are defined in the form below:

$$\lambda = \frac{m\pi}{\kappa_x}, \quad \delta = \frac{n\pi}{\kappa_y \varepsilon}, \quad \beta = \sqrt{\lambda^2 + \delta^2}$$

$$A_0 = \frac{s_{00}^t}{\varepsilon} = \frac{s_{00}^b}{\varepsilon}$$

$$A_m = \frac{2}{\varepsilon\lambda}\left(s_{m0}^b \operatorname{csch}(\lambda\varepsilon_H) - s_{m0}^t \coth(\lambda\varepsilon_H)\right)$$

$$A_n = \frac{2}{\varepsilon\delta}\left(s_{0n}^b \operatorname{csch}(\delta\varepsilon_H) - s_{0n}^t \coth(\delta\varepsilon_H)\right)$$

$$A_{mn} = \frac{4}{\varepsilon\beta}\left(s_{mn}^b \operatorname{csch}(\beta\varepsilon_H) - s_{mn}^t \coth(\beta\varepsilon_H)\right)$$

$$B_m = \frac{2s_{m0}^t}{\varepsilon\lambda} \quad B_n = \frac{2s_{0n}^t}{\varepsilon\delta} \quad B_{mn} = \frac{4s_{mn}^t}{\varepsilon\beta}$$

In which the auxiliary coefficients "s"s are

$$s_{00}^{t\,\mathrm{or}\,b} = \iint_{t\,\mathrm{or}\,b} q_{i(x,y)}^* dx^* dy^*$$

$$s_{m0}^{t\,\mathrm{or}\,b} = \iint_{t\,\mathrm{or}\,b} q_{i(x,y)}^* \times \cos(\lambda\kappa_x x^*) dx^* dy^*$$

$$s_{0n}^{t\,\mathrm{or}\,b} = \iint_{t\,\mathrm{or}\,b} q_{i(x,y)}^* \times \cos\left(\delta\kappa_y y^*\right) dy^* dx^*$$

$$s_{mn}^{t\,\mathrm{or}\,b} = \iint_{t\,\mathrm{or}\,b} q_{i(x,y)}^* \times \cos(\lambda\kappa_x x^*) \cos\left(\delta\kappa_y y^*\right) dx^* dy^*$$

References

[1] Gurrum, S. P., Suman, S. K., Joshi, Y. K., and Fedorov, A. G., 2004, "Thermal Issues in Next-Generation Integrated Circuits," IEEE Trans. Device Mater. Reliab., **4**(4), pp. 709–714.

[2] McGlen, R. J., Jachuck, R., and Lin, S., 2004, "Integrated Thermal Management Techniques for High Power Electronic Devices," App. Therm. Eng., **24**(8–9), pp. 1143–1156.

[3] Zuo, Z., Hoover, L. R., and Phillips, A. L., 2002, "Advanced Thermal Architecture for Cooling of High Power Electronics," IEEE Trans. Compon. Packag. Technol., **25**(4), pp. 629–634.

[4] Wunderle, B., and Michel, B., 2006, "Progress in Reliability Research in the Micro and Nano Region," Microelectron. Reliab., **46**(9–11), pp. 1685–1694.

[5] Suhir, E., 2013, "Thermal Stress Failures in Electronics and Photonics: Physics, Modeling, Prevention," J. Therm. Stresses, **36**(6), pp. 537–563.

[6] Suhir, E., Shangguan, D., and Bechou, L., 2013, "Predicted Thermal Stresses in a Trimaterial Assembly With Application to Silicon-Based Photovoltaic Module," ASME J. Appl. Mech., **80**(2), p. 021008.

[7] Kakaç, S., and Yener, Y., 1993, "One-Dimensional Steady-State Heat Conduction," *Heat Conduction*, 3rd ed., Taylor & Francis, Washington, DC, pp. 45–93.

[8] Moghaddam, S., Rada, M., Shooshtari, A., Ohadi, M., and Joshi, Y., 2003, "Evaluation of Analytical Models for Thermal Analysis and Design of Electronic Packages," Microelectron. J., **34**(3), pp. 223–230.

[9] Luo, X., Mao, Z., Liu, J., and Liu, S., 2011, "An Analytical Thermal Resistance Model for Calculating Mean Die Temperature of a Typical BGA Packaging," Thermochim. Acta, **512**(1–2), pp. 208–216.

[10] Liu, S., Leung, B., Neckar, A., Memik, S. O., Memik, G., and Hardavellas, N., 2011, "Hardware/Software Techniques for DRAM Thermal Management," IEEE 17th International Symposium on High Performance Computer Architecture (HPCA), San Antonio, TX, February 12–16, pp. 515–525.

[11] Zhao, R., Gosselin, L., Fafard, M., and Ziegler, D. P., 2013, "Heat Transfer in Upper Part of Electrolytic Cells: Thermal Circuit and Sensitivity Analysis," Appl. Therm. Eng., **54**(1), pp. 212–225.

[12] El-Nasr, A. A., and El-Haggar, S. M., 1996, "Effective Thermal Conductivity of Heat Pipes," Heat Mass Transfer, **32**(1–2), pp. 97–101.

[13] Zuo, J., and Faghri, A., 1998, "A Network Thermodynamic Analysis of the Heat Pipe," Int. J. Heat Mass Transfer, **41**(11), pp. 1473–1484.

[14] Shabgard, H., and Faghri, A., 2011, "Performance Characteristics of Cylindrical Heat Pipes With Multiple Heat Sources," Appl. Therm. Eng., **31**(16), pp. 3410–3419.

[15] Romary, F., and Caldeira, A., 2011, "Thermal Modelling to Analyze the Effect of Cell Temperature on PV Modules Energy Efficiency," 14th European Conference on Power Electronics and Applications (EPE 2011), Birmingham, UK, August 30–September 1.

[16] Del Valle, P. G., and Atienza, D., 2011, "Emulation-Based Transient Thermal Modeling of 2D/3D Systems-on-Chip With Active Cooling," Microelectron. J., **42**(4), pp. 564–571.

[17] Barcella, M., Huang, W., Skadron, K., and Stan, M., 2002, "Architecture-Level Compact Thermal R-C Modeling," Department of Electrical and Computer Engineering, University of Virginia, Charlottesville, VA, Technical Report No. CS-2002-20.

[18] Stan, M. R., Skadron, K., Barcella, M., Huang, W., Sankaranarayanan, K., and Velusamy, S., 2003, "HotSpot: A Dynamic Compact Thermal Model at the Processor-Architecture Level," Microelectron. J., **34**(12), pp. 1153–1165.

[19] Magnone, P., Fiegna, C., Greco, G., Bazzano, G., Rinaudo, S., and Sangiorgi, E., 2013, "Numerical Simulation and Modeling of Thermal Transient in Silicon Power Devices," Solid-State Electron., **88**, pp. 69–72.

[20] Cova, P., Bernardoni, M., Delmonte, N., and Menozzi, R., 2011, "Dynamic Electro-Thermal Modeling for Power Device Assemblies," Microelectron. Reliab., **51**(9–11), pp. 1948–1953.

[21] López-Walle, B., Gauthier, M., and Chaillet, N., 2010, "Dynamic Modelling for Thermal Micro-Actuators Using Thermal Networks," Int. J. Therm. Sci., **49**(11), pp. 2108–2116.

[22] Miana, M., and Cortés, C., 2010, "Transient Thermal Network Modeling Applied to Multiscale Systems. Part II: Application to an Electronic Control Unit of an Automobile," IEEE Trans. Adv. Packag., **33**(4), pp. 938–952.

[23] Miana, M., and Cortés, C., 2010, "Transient Thermal Network Modeling Applied to Multiscale Systems. Part I: Definition and Validation," IEEE Trans. Adv. Packag., **33**(4), pp. 924–937.

[24] Ramallo-González, A. P., Eames, M. E., and Coley, D. A., 2013, "Lumped Parameter Models for Building Thermal Modelling: An Analytic Approach to Simplifying Complex Multi-Layered Constructions," Energy Build., **60**, pp. 174–184.

[25] Buonomano, A., and Palombo, A., 2014, "Building Energy Performance Analysis by an In-House Developed Dynamic Simulation Code: An Investigation for Different Case Studies," Appl. Energy, **113**, pp. 788–807.

[26] Athienitis, A., Kalogirou, S. A., and Candanedo, L., 2012, "Modeling and Simulation of Passive and Active Solar Thermal Systems," *Comprehensive Renewable Energy*, Vol. 3: Solar Thermal Systems: Components and Applications, Elsevier, Ltd., Amsterdam, Netherlands, pp. 357–417.

[27] Gholami, A., and Bahrami, M., 2014, "Spreading Resistance in Anisotropic Rectangular Plates With Multiple Heat Sources and Sinks," 10th International Conference on Heat Transfer, Fluid Mechanics, and Thermodynamics, Orlando, FL, July 14–16.

[28] Ferrandi, C., Iorizzo, F., Mameli, M., Zinna, S., and Marengo, M., 2013, "Lumped Parameter Model of Sintered Heat Pipe: Transient Numerical Analysis and Validation," Appl. Therm. Eng., **50**(1), pp. 1280–1290.

[29] Zhu, N., and Vafai, K., 1999, "Analysis of Cylindrical Heat Pipes Incorporating the Effects of Liquid-Vapor Coupling and Non-Darcian Transport—A Closed Form Solution," Int. J. Heat Mass Transfer, **42**(18), pp. 3405–3418.

[30] Mostafavi, G., 2013, "Effect of Fin Interruptions on Natural Convection Heat Transfer From a Rectangular Interrupted Single-Wall," ASME Paper No. IPACK2013-73129.

[31] Dede, E., 2012, "Optimization and Design of a Multipass Branching Microchannel Heat Sink for Electronics Cooling," ASME J. Electron. Packag., **134**(4), p. 041001.

[32] Xie, G., and Liu, J., 2012, "Analysis of Flow and Thermal Performance of a Water-Cooled Transversal Wavy Microchannel Heat Sink for Chip Cooling," ASME J. Electron. Packag., **134**(4), p. 041010.

[33] Xie, G., Liu, J., and Liu, Y., "Comparative Study of Thermal Performance of Longitudinal and Transversal-Wavy Microchannel Heat Sinks for Electronic Cooling," ASME J. Electron. Packag., **135**(2), p. 021008.

[34] Xie, G., Zhang, F., Sundén, B., and Zhang, W., 2014, "Constructal Design and Thermal Analysis of Microchannel Heat Sinks With Multistage Bifurcations in Single-Phase Liquid Flow," Appl. Therm. Eng., **62**(2), pp. 791–802.

[35] Incropera, F., DeWitt, D., Bergrnan, T., and Lavine, A. S., 2007, *Fundamentals of Heat and Mass Transfer*, 6th ed., Wiley, Hoboken, NJ, pp. 559–780.

Downloaded From: http://turbomachinery.asmedigitalcollection.asme.org/ on 04/13/2015 Terms of Use: http://asme.org/terms